Journal of Alloys and Compounds 495 (2010) 408–411

Contents lists available at ScienceDirect

Journal of Alloys and Compounds

journal homepage: www.elsevier.com/locate/jallcom

Small-angle X-ray scattering study of the early stages of precipitation in a Mg–Nd–Gd (EV31) alloy

Rafael Ferragut[a,*], Fabio Moia[a], Fabrizio Fiori[b], Danilo Lussana[c], Giuseppe Riontino[c]

[a] Dipartimento di Fisica, LNESS and CNISM, Politecnico di Milano, via Anzani 42, I-22100 Como, Italy
[b] Dipartimento SAIFET - Sezione di Scienze Fisiche and CNISM - Laboratorio MATEC, Università Politecnica delle Marche, via Brecce Bianche, I-60131 Ancona, Italy
[c] Dipartimento di Chimica I.F.M., N.I.S. Centre and CNISM, Università di Torino, via Giuria 9, I-10125 Torino, Italy

ARTICLE INFO

Article history:
Received 31 July 2008
Received in revised form 14 October 2009
Accepted 15 October 2009
Available online 24 October 2009

Keywords:
Metals and alloys
Nanostructured materials
Precipitation
Microstructure
Small-angle X-ray scattering (SAXS)

ABSTRACT

A quantitative description of the Mg-rare earth EV31 alloy during the first stages of the precipitation sequence using *in situ* small-angle X-ray scattering (SAXS) is presented. *In situ* evolutions of the size, volume fraction and number density of precipitates formed at 150 °C and 200 °C were obtained. A kinetic mechanism suggests that the precursor nanoparticles are nucleated at the beginning of the artificial ageing and, at 200 °C, these particles grow mainly by accretion of the solute from the matrix without further nucleation. The particles grow within two regimes: (i) at the beginning of ageing, the growth is associated with solute diffusion with an apparent activation energies of 0.78 eV (diffusion assisted by vacancies); (ii) further growth is associated with solute diffusion with an apparent activation energies of 1.16 eV (bare solute diffusion). After about 2 h at 200 °C, corresponding to the condition of maximum hardness for this alloy, the present results indicate a volume fraction of about 1.5% occupied by particles with an average Guinier radius of 2 nm. The evolution of the volume fraction at 150 °C, studied for a similar time interval, is weaker than the one found at 200 °C.

1. Introduction

The Mg-rare earth EV31 alloy (Elektron 21) has been recently introduced into the aerospace industry because of its improved corrosion resistance and reduced production costs [1]. This alloy, which has properties similar to WE43 alloy, was formally launched in Europe and USA in 2003. An effective and exhaustive report on the influence of alloying elements upon the properties of EV31 has been made by Lyon et al. [2]. Recent studies performed on alloys having compositions similar to EV31 have evidenced the importance of small additions of Zn in the age-hardening response [3], while direct observations by 3-D atom probe made it possible to characterize the composition of nanoscale precipitates in a similar alloy [4].

A previous microstructural characterization of EV31 at different temperatures by means of hardness measurements, DSC, TEM and positron annihilation spectroscopy was performed in Ref. [5]. In the present work a quantitative description of the first stages of the precipitation sequence using *in situ* small-angle X-ray scattering (SAXS) is presented. The new information suggests a precipitation mechanism for the nucleation and growth of the nanoparticles.

2. Experimental details

Extruded bars of nominal composition Mg, 2.8Nd, 1.4Gd, 0.3Zn, 0.5Zr (wt.%), corresponding to Mg, 0.49Nd, 0.23Gd, 0.12Zn, 0.14Zr (at.%) were supplied by Teksid Aluminum in the as-cast conditions. Small discs of about 5 mm in diameter and about 0.1–mm thick were prepared for SAXS measurements. These samples were solution treated for 8 h at 525 °C in a vertical furnace, then quenched in water at room temperature.

SAXS experiments were performed at ESRF (beamline BM02) at the fixed X-ray wavelength $\lambda = 1$ Å, in the range of the scattering vector modulus 1.6×10^{-2} Å$^{-1} < q < 0.6$ Å^{-1} ($q = 4\pi \sin(\theta/2)/\lambda$, θ being the scattering angle). The 2-D spectrum was circularly averaged to obtain the 1-D spectrum $I(q)$, which was calibrated by comparison with the spectrum measured in the same conditions for a reference sample. The data were corrected for a flat background and diffuse multiple scattering from the matrix (Porod correction, see Ref. [6]).

The data treatment yields the Guinier radius, R_G, and the integrated intensity

$$Q_0 = \int_0^\infty q^2 I(q)\, dq = Q^{s.a.} + Q^{meas.} + Q^{w.a.} \quad (1)$$

Q_0 is determined as the sum of three terms $Q^{s.a.} + Q^{meas.} + Q^{w.a.}$, where $Q^{s.a.}$ is the contribution due to scattering at very small angles (below the minimum angle experimentally reachable), $Q^{w.a.}$ the area at wide angles extended beyond the maximum measured angle and Q^{meas} is the main part of the integral that can actually be measured (see Ref. [6]). The average Guinier radius, R_G, is obtained from the plot $I(q)q^2$ vs. q, which, if the Guinier approximation holds, has a maximum at $q_G = \sqrt{3}/R_G$. In the framework of the "two-phase model", Q_0 is related to the volume fraction f_V occupied by the scattering centres, according to the equation:

$$Q_0 = 2\pi^2 |\Delta\rho|^2 f_V (1 - f_V) \quad (2)$$

* Corresponding author. Tel.: +39 0313327338; fax: +39 0313327617.
E-mail address: rafael.ferragut@polimi.it (R. Ferragut).

0925-8388/$ – see front matter © 2009 Elsevier B.V. All rights reserved.
doi:10.1016/j.jallcom.2009.10.111

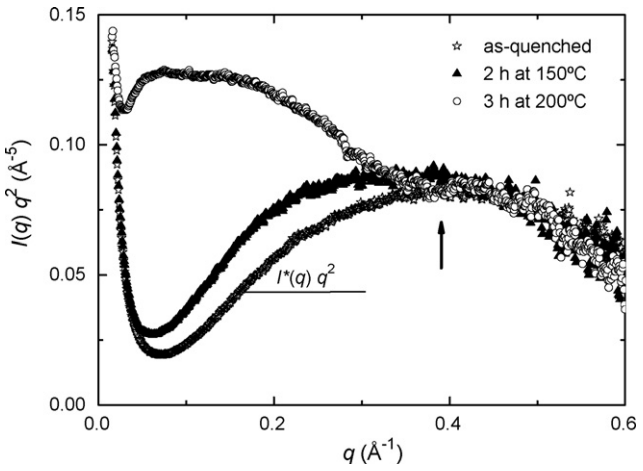

Fig. 1. Plot of $I(q)\ q^2$ vs. q SAXS profile measured after solution treatment and quenching ($I^*(q)\ q^2$), 2 h at 150 °C and 3 h at 200 °C.

where $\Delta\rho$ is the average electron density difference between the scattering centres and the matrix. Neglecting the residual content of solute in the matrix, one can write

$$\Delta\rho = \frac{\bar{Z}_p}{\Omega_p} - \frac{\bar{Z}_m}{\Omega_m} \approx \frac{\bar{Z}_p - Z_{Mg}}{\Omega} \quad (3)$$

where $\bar{Z}_p$, $\bar{Z}_m$ are the average atomic numbers respectively in the scattering centres and in the matrix, Ω_p and Ω_m the atomic volumes in the scattering centres and in the matrix. $\Omega = 23.2$ Å^3 is a rather accurate approximation for $\Omega_p \approx \Omega_m$ [7]. The composition of the precipitates was calculated under the hypothesis that particles with a DO_{19} structure (β″ phase) are formed during the first stages of precipitation in agreement with the results given in Ref. [5]. Under this hypothesis, it is then possible to follow the evolution of volume fraction f_V with increasing ageing time, by comparing their integrated intensity. An estimate of f_V can be obtained by neglecting second-order terms in Eq. (2); this approximation gives

$$f_V = \alpha Q_0 \quad (4)$$

The composition proposed for the β″ phase is Mg_3X, where X are rare earths (Nd, Gd or a balance between these elements). In Eq. (4), the constant α was estimated in 0.175 Å^6 with a balance in the composition of the β″ phase Nd/Gd = 1 (α = 0.161 Å^6 if X = Gd and α = 0.189 Å^6 if X = Nd). Therefore, Eq. (4) gives an estimation of the volume fraction, since at present the exact composition and a possible variation of this during ageing is not known. Assuming that spherical particles are formed at the beginning of artificial ageing, the number density of the scattering centres can be estimated by the relationship

$$n = \frac{f_V}{4/3\pi R^3} = \frac{f_V}{4/3\pi(5/3)^{3/2}R_G^3} \cong 1.95 \times 10^{-2}\ \text{Å}\ \frac{Q_0}{R_G^3} \quad (5)$$

More details about the SAXS technique can be found in Refs. [8,9].

3. Results and discussion

Fig. 1 shows the $I(q)q^2$ vs. q distribution after solution treatment and quenching and at the interruption of the ageing treatments (2 h at 150 °C and 3 h at 200 °C). The distribution shows a bump for high value of q with a maximum indicated by an arrow, which seems to reveal the persistent presence of very fine objects within the magnesium matrix. The average Guinier radius of these hypothetical particles would be about 4.5 Å and their volume fraction would be around 1%. The comparison of the three curves in Fig. 1 indicates that the right side of the bump associated with these particles does not change significantly after artificial ageing for the entire duration of our experiment. The nature of these particles is not easily explainable in terms of the precipitation process studied in the present work. However, in accordance with the results of atom probe tomography for Al–Cu–Mg alloys [10,11], it seems reasonable to attribute the initial distribution to solute clusters or co-clusters (clusters with more than one atomic species) containing only a few solute atoms. For the temperatures and ageing times explored in the present experiment, this distribution does not seem substantially depleted. If the solute clusters contribute as a reserve

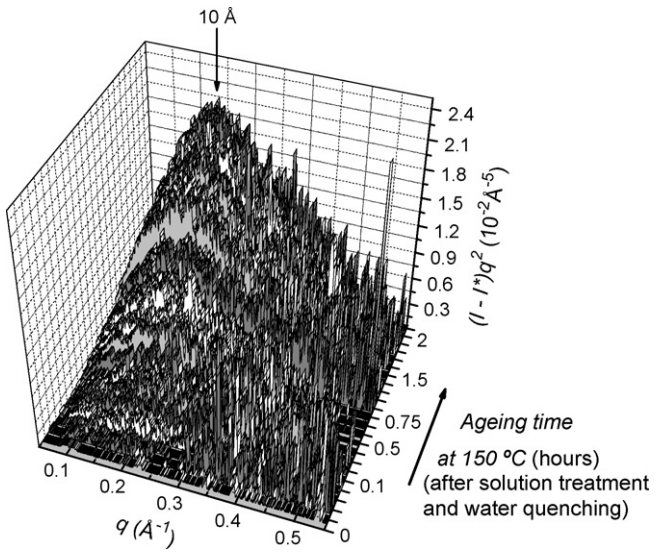

Fig. 2. *In situ* SAXS distribution measured at 150 °C of alloy EV31.

of solute for the formation of new precipitates, only a few percent of these clusters have been used. Particles formed with minor alloy elements during solidification that are stable during artificial ageing could also be present (see peritectic Zr-rich particles in Ref. [12]). In order to obtain information on the size and density of the new particles formed during ageing, the contribution to the scattered intensity of the small clusters already present immediately after quenching needs to be subtracted. In our approximated analysis, we assume that this contribution remains unchanged during ageing.

Figs. 2 and 3 show the *in situ* evolution of the SAXS distribution $(I - I^*)q^2$ during the first hours obtained at 150 °C and 200 °C, where $I(q)$ is the scattering intensity measured at different ageing stages and $I^*(q)$ the intensity measured for solution treated and quenched samples (Fig. 1). The area under the curves (integrated intensity) is proportional to the volume fraction of the new particles formed during the evolution and the position of the maximum is inversely proportional to their size. It is evident that the distribution at 150 °C is much less developed than at 200 °C. Figs. 2 and 3 also show that there is a q spread up to 0.5 Å^{-1} and 0.32 Å^{-1}, corresponding to a

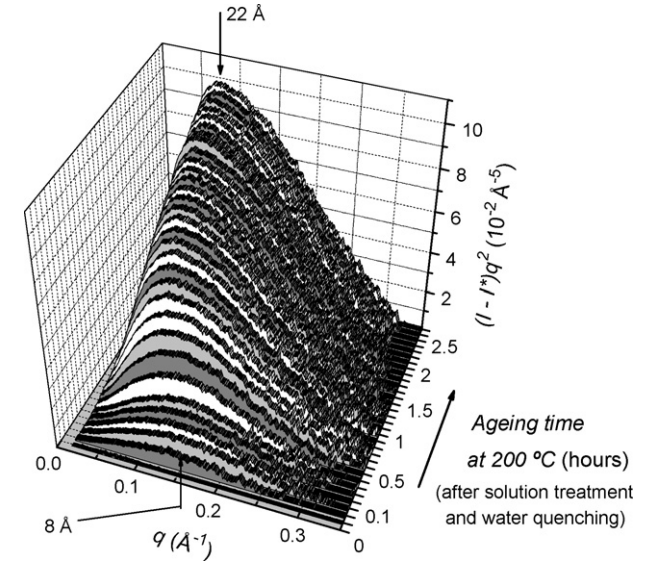

Fig. 3. *In situ* SAXS distribution measured at 200 °C of alloy EV31.

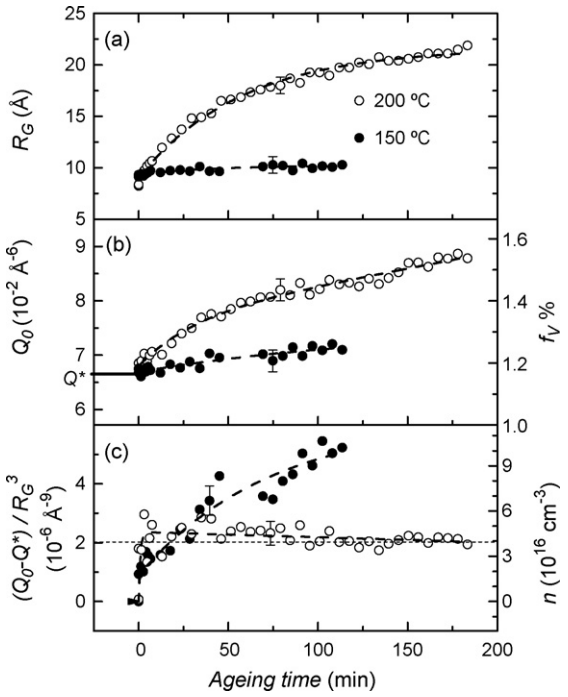

Fig. 4. *In situ* evolution of the SAXS results during artificial ageing. (a) Guinier radius, R_G; (b) integrated intensity Q_0 (left axis) and approximated volume fraction f_V of precipitates (right axis); (c) ratio $(Q_0 - Q^*)/R_G^3$ (left axis) and approximated number density of precipitates (right axis). Typical error bars shown for one point only in each frame.

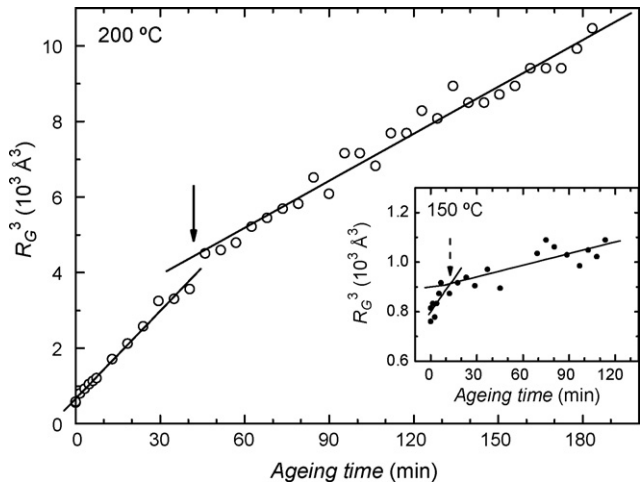

Fig. 5. Variation of the cube of the average particle Guinier radius as a function of ageing time. The evolution at 150 °C is included into the insert with different scales.

Guinier radius of 3.5 Å and 5.4 Å, respectively. The different spread in the scattering distributions is an approximated indication of the temperature dependence of the lower size limit for the thermal stability of the new particles.

Fig. 4 shows the evolution of the Guinier radius R_G, the integrated intensity Q_0 and the ratio $(Q_0 - Q^*)/R_G^3$ at 150 °C and 200 °C. The scales on the right show the volume fraction and the number density of the scattering centres, evaluated according to Eqs. (4) and (5). The dashed lines through the experimental points are only a guide for the eye. Fig. 4a shows an initial Guinier radius value of about 8–9 Å of the new particles that are nucleated at both temperatures immediately after the beginning of the artificial ageing. After 2 h at 150 °C there is a small R_G increase. On the contrary, at 200 °C there is a substantial growth of the particles up to a non-saturated maximum of about 22 Å at the interruption of the measurement. This analysis was performed on the hypothesis that during the first stages of precipitation three-dimensional particles are formed in good agreement with the TEM evaluation of Ref. [5]. The Porod radius R_p (see Ref. [8]) when calculated with the whole $I(q)$ distribution (Fig. 1) practically does not change during the evolution (between 3.3 Å and 4.4 Å). This Porod radius is highly influenced by the initial distribution of small particles, which has no strong evolution during the ageing. Fig. 4b, which shows the evolution of the integrated intensity Q_0 (thus the volume fraction), includes the contribution of the small clusters. This contribution is subtracted in Fig. 4c, showing the evolution of $(Q_0 - Q^*)/R_G^3$, which is proportional to the number density n of the new particles that are formed during artificial ageing. The variation of n is small at both temperatures in comparison to number density of the small particles present at the beginning of the ageing (2×10^{18} particles/cm^3). At 150 °C, n increases up to a non-saturated maximum at the interruption of the measurement. At 200 °C one observes a rapid increase, followed by a smooth decrease with possible saturation at a value three times smaller than the maximum reached at 150 °C. The increase of the number of particles is an indication of nucleation that takes place immediately after the beginning of artificial ageing; the behaviour at longer ageing times at 200 °C is symptomatic of accretion of the solute aggregates without further nucleation.

The precipitation mechanism observed during the early stages of ageing can be summarized as follows: (i) nucleation occurs at the beginning of the thermal treatment at both temperatures (150 °C and 200 °C); (ii) at 200 °C, continuing growth of particles by the absorption of solute from the matrix appears to be energetically favoured than the nucleation of new particles.

Fig. 5 shows that the volume of the new particles (R_G^3) grows in proportion to the ageing time within two regimes (the insert depicts the evolution at 150 °C with a different scale). The more rapid regime takes place below about 10 min at 150 °C and about 40 min at 200 °C. A linear R_G^3 -time law is reminiscent of a coarsening process described by the LSW (Lifshitz–Slyozov–Wagner) model, which in this case seems to hold even in a stage where nucleation is still taking place. This has been previously observed in other cases (see an example in Ref. [13]). There is currently a lack of data of diffusion rates of rare earths in magnesium in the literature. We thus follow the procedure of Ref. [13] to estimate the activation from temperature dependence of the slopes of the lines in Fig. 5. For the rapid regime, the activation energy can be evaluated at (0.78 ± 0.15) eV (75 kJ/mol). This energy must be associated with solute migration (Gd and Nd). The atomic sizes of both Gd and Nd (~1.8 Å in radius [14]) are larger than that of Mg (1.6 Å) and is most likely that their diffusion is assisted by associated vacancies The presence of vacancies in association to isolated solute atoms and to small solute aggregates formed at the beginning of ageing can be expected to minimize the internal energy. The estimated activation energy is in accordance with the value obtained by Zhu and Nie [15] in a Mg–Y–Nd alloy by means of serrated flow, which was associated with the diffusion of rare earth atoms (Y and Nd) in Mg. For the slower growth regime, the activation energy is estimated at (1.16 ± 0.12) eV (112 kJ/mol). This value, which is slightly lower than the activation energy of Mg self-diffusion (1.39 eV ≡ 134 kJ/mol) [16], is likely to be associated with bare solute (Gd and/or Nd) diffusion in Mg.

The condition of maximum strength (hardness) for the EV31 alloy [5] was found in artificially aged samples for about 2 h at 200 °C. The results presented in the present work indicate that in this condition particles of 2 nm with a volume fraction of about 1.5% are found. TEM observations of Ref. [5] for a longer ageing exposition, i.e. after 1 day at 150 °C and 16 h at 200 °C, reveal the presence of small platelets about 4 nm and 12 nm in diameter, respectively. Such particles were associated with the formation of the chemically

ordered DO19 structure that doubles the hexagonal Mg base cell ($a = 2a_{Mg}$, $c = c_{Mg}$), i.e. the coherent β″ phase that has a composition Mg_3X (X = rare earth).

4. Conclusions

The present work contributes to the characterization of the new Mg alloy EV31 by presenting a quantitative description of the first stages of the precipitation sequence using *in situ* small-angle X-ray scattering. The proposed main mechanism of precipitation kinetic suggests that: (i) the coherent particles of the β″ phase or precursors of this phase are nucleated mainly during the first minutes of ageing; (ii) the particles reach an approximated critical diameter larger than 7 Å and 11 Å, below which they are thermally unstable at 150 °C and 200 °C, respectively; (iii) growth of the particles takes place by absorption of the solute from the matrix in two stages with different activation energies (0.78 ± 0.15) eV and (1.16 ± 0.12) eV associated with the diffusion of solute with or without vacancies.

Artificial hardening at 200 °C was shown to be faster and more efficient than for the suggested commercial T6 temper (16 h at 200 °C) [1]. The hardness maximum was previously found at about 2 h [5]. The present work points out that in these conditions there is a distribution of solute aggregates with an average Guiner radius of 2 nm and a volume fraction of 1.5%. It is reasonable to assume that the particles are precipitates of the β″ phase, although to our knowledge there is no available conventional electron microscopy identification of the precipitates in these early ageing conditions.

Acknowledgements

The authors acknowledge the support of ESRF for the SAXS measurements (beamline BM02-D2AM) and, in particular, the assistance of Dr. Françoise Bley. We thank Prof. A. Dupasquier for critically reading the manuscript and making several useful remarks.

References

[1] Magnesium Elektron, datasheet no. 455, www.magnesium-elektron.com.
[2] P. Lyon, T. Wilkis, I. Syed, TMS Magnesium Technol. (2005) 303.
[3] J.F. Nie, X. Gao, S.M. Zhu, Scripta Mater. 23 (2005) 1049.
[4] D.H. Ping, K. Hono, J.F. Nie, Scripta Mater. 48 (2003) 1017.
[5] G. Riontino, D. Lussana, M. Massazza, G. Barucca, P. Mengucci, R. Ferragut, J. Alloys Compd. 463 (2008) 200.
[6] A. Dupasquier, R. Ferragut, M.M. Iglesias, M. Massazza, G. Riontino, P. Mengucci, G. Barucca, C.E. Macchi, A. Somoza, Philos. Mag. 87 (2007) 3297.
[7] C. Antion, P. Donnadieu, F. Perrard, A. Deschamps, C. Tassin, A. Pisch, Acta Mater. 51 (2003) 5335.
[8] O. Glatter, O. Kratky, Small-angle X-ray Scattering, Academic Press, London, 1982.
[9] A. Guinier, G. Fournet, Small-angle Scattering of X-rays, Wiley, New York, 1955.
[10] R.K.W. Marceau, G. Sha, R. Ferragut, A. Dupasquier, S.P. Ringer, Acta Mater., submitted for publication.
[11] R.K.W. Marceau, Ph.D. thesis, The University of Sydney, 2008.
[12] E.F. Emley, Principles of Magnesium Technology, Pergamon Press, Oxford, 1966.
[13] Z. Du, T. Zhou, P. Liu, H. Li, B. Dong, C. Chen, J. Mater. Sci. Technol. 21 (2005) 479.
[14] L.L. Rokhlin, Magnesium Alloys Containing Rare Earth Metals: Structure and Properties, Taylor & Francis, London, 2003.
[15] S.M. Zhu, J.F. Nie, Scripta Mater. 50 (2004) 51.
[16] M. Bamberger, G. Dehm, Annu. Rev. Mater. Res. 38 (2008) 505.